Plasma Sources Science and Technology

ACCEPTED MANUSCRIPT

Understanding the depletion of electrons in dusty plasmas at atmospheric pressure

To cite this article before publication: Nabiel Hilmy Abuyazid *et al* 2020 *Plasma Sources Sci. Technol.* in press https://doi.org/10.1088/1361-6595/ab9cc3

Understanding the depletion of electrons in dusty plasmas at atmospheric pressure

Nabiel H. Abuyazid[1], Xiaoshuang Chen[2], Davide Mariotti[3], Paul Maguire[3], Christopher J. Hogan Jr.[2] and R. Mohan Sankaran[1]*

1. Department of Chemical and Biomolecular Engineering

Case Western Reserve University, Cleveland OH 44106, USA

2. Department of Mechanical Engineering

University of Minnesota, Minneapolis MN 55455

3. Nanotechnology and Integrated Bioengineering Center (NIBEC)

Ulster University, Newtownabbey, UK BT37 0QB

* To whom correspondence should be addressed:

E-mail address: mohan@case.edu

Abstract

The nucleation and growth of nanoparticles in the gas phase using atmospheric-pressure plasma systems is an important approach to synthesizing novel dimensionally-controlled materials. Here, we investigated the effect of the nanoparticles on a typical type of continuous-flow, substrate-free plasma at atmospheric pressure to understand their potential contribution to electron density changes. A tandem plasma system was set up consisting of one plasma reactor that produced carbonaceous nanoparticles from mixtures of argon and hexane, and another identical plasma reactor where the as-grown particles were injected and non-intrusive electrical and optical measurements were performed. The electron densities obtained from conductivity measurements and a plasma fluid model were found to decrease in the presence of nanoparticles. However, control experiments revealed that the main source of the electron depletion was residual vapor or small molecule products (nanoclusters) and not the particles themselves. These results were validated by constant number Monte Carlo simulations which showed that at the experimentally-measured conditions, the nanoparticles were not of sufficiently high enough concentration to reduce the electron density; however, if residual vapor molecules and clusters are ionizable, they remain in sufficient concentration to deplete electron densities when compared to pristine plasma densities. Our study shows that at atmospheric pressure, because of their typically larger electron density values, particle-producing plasmas are distinct from those at low pressure, and nanoparticle formation does not have the same impact while molecular-scale species may be a more important consideration.

I. Introduction

Nanoparticle formation by homogeneous, gas-phase nucleation using low-temperature plasmas has evolved from an undesired issue during chemical vapor deposition of thin films [1] to a viable synthesis strategy for a broad range of dimensionally-controlled materials [2]. Fundamentally, these particle-producing plasmas are multiphase systems composed of solid particle and plasma phases engaging in complex coupled phenomena. At a simple level, there are two main effects: i) how the plasma influences particle formation and ii) how the growing particles affect plasma properties. Most recent research efforts have focused on addressing particle formation, specifically controlling nanoparticle properties for their intended applications such as size, composition, morphology, and crystallinity [3,4].

The effect of particles on plasma properties has been historically studied by dusty plasma experiments where larger, micrometer-sized, pre-existing particles are introduced into a low-pressure plasma [5,6]. Among the various types of plasma-particle interactions, the most obvious is perhaps particle charging by collisions of nanoparticles with the charged plasma species, typically negatively-charged electrons and positively-charged ions [7–9]. The charging of particles leads to several cumulative effects. Particles will preferentially charge negatively in a plasma because of the higher mobilities and lower masses of electrons as compared to ions. The attachment of electrons to particles concomitantly reduces the plasma (electron) density, which could impact stability or in extreme cases, extinguish the plasma [7]. As a result of the negative charging, the particles will have a negative floating potential in the plasma and be subjected to fluxes of ions and electrons to their surface. Among various surface processes, ion-electron recombination on or near the surface can release substantial amounts of energy (*e.g.*, 15.6 eV for argon, Ar) [4]. Consequently, nanoparticles can be selectively heated to temperatures well above the gas

temperature in the plasma, which may explain the formation of crystalline materials of high melting point such as silicon [10,11]. Nanoparticles can also evaporate as a result of the ion flux to their surface and the vapor produced can re-nucleate particles, causing overall a size-focusing of the particle population [12].

Several recent efforts have been aimed at more carefully characterizing plasma-particle interactions in realistic particle-producing environments, and in particular, measuring the electron density and charge on particles. *In situ* Langmuir probe measurements of a low-pressure plasma during nucleation and growth of silicon nanoparticles showed a decrease in the electron density resulting from electron attachment to the particles [13]. To eliminate the interfering effect of dust-forming chemistry on Langmuir probe, a tandem low-pressure, flowing plasma system was developed made up of one plasma to synthesize nanoparticles by gas-phase nucleation, and another, but not identical, to introduce the particles and apply diagnostics. Again, Langmuir probe measurements confirmed that electrons are depleted in the presence of particles [14]. While these various effects of particles on the plasma have been shown, all of these studies have been carried out at low (sub-atmospheric) pressures and it is not yet known if the same effects occur in atmospheric pressure plasmas, which occupy an important area of particle-producing plasma systems [15].

Here, we present a fundamental study of plasma-particle interactions at atmospheric pressure. We designed a flow-through, tandem system consisting of two identical atmospheric-pressure argon plasmas of the type that have been previously used to synthesize nanoparticles by gas-phase nucleation [16,17]. Carbonaceous nanoparticles were synthesized in the first plasma from dilute mixtures of hexane vapor in Ar, and continuously introduced into the second plasma where plasma and particle characterization were performed. A critical challenge for atmospheric-

pressure plasmas is that Langmuir probe and other contact-based diagnostics are challenged because of the small size of the plasmas and the collisionality at high pressures. For this reason, non-contact methods were applied based on electrical characteristics and optical emission spectroscopy (OES). Our measurements indicated that the electron density decreased in the atmospheric-pressure plasma upon introduction of a nanoparticle-laden flow, as might be expected from the preferential electron charging of particles. However, control experiments based on filtering the particles revealed that the sink for electron depletion was either unreacted vapor precursor or molecular products from the reactive plasma. Constant number Monte Carlo simulations [18] using recently developed collision rate coefficients for ion-particle collisions in an intermediate collisional regime [19,20] were carried out in support of the experiments and confirmed that under our environmental conditions, the nanoparticles do not appreciably alter the electron density. Overall, these results are in stark contrast to previous studies on low-pressure plasmas and indicate that the impact of nanoparticles at atmospheric pressure is less substantive, especially in comparison to molecular species.

II. Methods

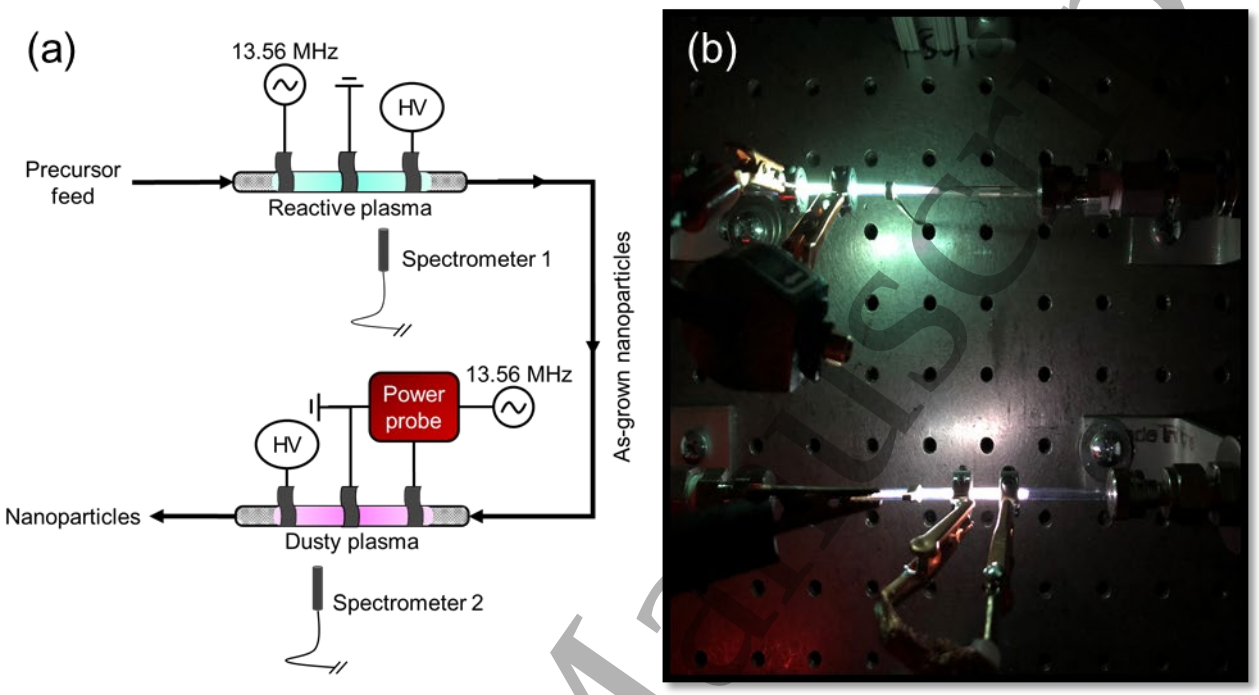

Figure 1. (a) Schematic diagram of tandem atmospheric-pressure plasma system, and **(b)** corresponding image of "reactive" (top) and "dusty" (bottom) atmospheric-pressure plasmas during standard particle-containing operation.

A tandem, flow-through plasma system was designed and constructed to study plasma-particle interactions in a realistic, atmospheric-pressure plasma environment. The setup, schematically illustrated with an accompanying photo in Fig. 1, consisted of two identical radio frequency (RF)-powered, flowing plasmas formed inside quartz tubes (Quartz Scientific Inc., 2 mm I.D., 3 mm O.D.) with surrounding ring electrodes in a parallel configuration. There were three electrodes, each separated by 2 cm: one electrically connected to a RF power supply (RFVII RF-3 13.56 MHz) through a home-built L-type matching network (referred to as power), one connected to a high voltage AC power supply (Information Unlimited, Model PVM500-4000) (referred to as trigger), and one connected to electrical ground (referred to as ground). The plasmas were ignited by first applying AC voltage to the trigger electrode, and then sustained by applying

RF voltage to the powered electrode and turning off the AC voltage. The carrier gas was argon (Airgas Inc., industrial grade).

Nanoparticles were synthesized in the first plasma by introducing a vapor precursor, as has been previously reported for many different material chemistries [3,21]. We focused on carbonaceous nanoparticles and hexane as the vapor precursor, which is a liquid at room temperature, but has a sufficiently high vapor pressure. To control the vapor concentration, a gas stream of Ar was bubbled through hexane (Fisher Scientific, 98.5% purity) cooled to -15ºC, and this gas mixture was further diluted by another pure gas stream of Ar. Based on vapor-liquid equilibrium, the hexane precursor concentration in the plasma was 80 ppm in our experiments. During standard operation (referred to as "particle-containing" from this point forward), the as-grown carbonaceous nanoparticles were introduced into the second plasma where non-contact diagnostics were applied. The first plasma reactor is referred to as "reactive" and the second one as "dusty" for brevity. Control experiments were conducted in which the nanoparticles leaving the reactive plasma were removed by a filter (Parker Balston Model 9933-11) and only unreacted hexane or molecular reaction byproducts, if any, entered the second plasma.

The as-grown carbonaceous nanoparticles were characterized both online and offline. *In situ* characterization was performed via ion mobility spectrometry (IMS) using a commercial SMPS system consisting of a differential mobility analyzer (DMA, TSI Inc., Model 3085) and an ultrafine condensation particle counter (CPC, TSI Inc., Model 3776). Details of the operating principle of ion mobility spectrometry have been reported elsewhere [22]. Importantly, the nanoparticle-laden flow leaving the second plasma reactor was diluted with 1.3 lpm nitrogen (Airgas, industrial grade) to prevent arcing in the DMA during measurement. The DMA was operated with a recirculating sheath flow rate of 3.0 lpm and the CPC aspiration flow rate was 0.3

lpm. Prior to entering the DMA, the aerosol passed through a Kr-85 containing radioactive source, to bring particles to an initial-condition dependent steady-state charge distribution need for IMS-based size measurements. The TSI AIM software was used to control DMA-CPC scanning measurements and to invert nanoparticle size distributions from measurements. *Ex situ* characterization was performed by transmission electron microscopy (TEM). The nanoparticles were directly deposited onto 400 size, ultrathin carbon film with lacey carbon support, copper TEM grids (Ted Pella Inc.) by electrostatic precipitation using a commercial nanosampler (TSI Inc., Model 3089) to collect particles dry and minimize any morphological changes such as break up of aggregates. The nanosampler was modified to decrease the electrode gap to 1 cm and operated at -9 kV. The deposition time was 10 min.

Two non-contact methods were employed to characterize the dusty plasma. The first was electrical measurements using a RF power probe (Impedans Octiv Poly) in series with the power transmission to obtain the electron density. The electron density was estimated by measuring the discharge current and voltage and applying a simple plasma-fluid model which has been shown to be consistent with other diagnostic techniques [23]. Briefly, the charged species flux is expressed by the drift-diffusion approximation and the diffusive term is neglected. Assuming the contribution from ions is small in comparison to electrons because of the latter's higher mobility, the electron flux in the axial direction of a conductive cylindrical tube is related to the electron density, n_e, as the following [24,25]:

$$n_e = \frac{dI_g(t)}{Ae\mu_e V(t)} = \frac{d}{Ae\mu_e Z_p} \quad (1)$$

where $I_g(t)$ is the discharge current, A is the cross-sectional area, d is the electrode distance, μ_e is the electron mobility which for Ar at 760 Torr is 0.0681 $m^2 V^{-1} s^{-1}$ [25]), and I_p is the impedance of the plasma. The impedance is a complex number made up of a real component, which is the

resistance, and an imaginary component, which is the reactance. For the calculation of electron density, only the real, resistive component was used. Measuring the current while the plasma was on provided the total current in the system, and to separate the discharge current, a simple equivalent circuit model was developed for the plasma on and plasma off cases. In applying this model, we assumed that any temporal or spatial variations could be averaged and that the plasma sheath thickness at atmospheric pressure is small and negligible in comparison to the reactor geometry. Thus, the plasma could be approximated as a cylinder filling the gap between the electrodes and the inner diameter of the quartz tube. We note that the electron densities obtained from electrical probe measurements and the plasma-fluid model are volume-averaged quantities. Additional details of the plasma-fluid model are provided in the Supplementary Information.

The second non-contact method was optical emission spectroscopy (OES) using a broadband spectrometer (Ocean Optics HR4000, 0.5 nm resolution) to monitor precursor dissociation in the reactive plasma and a high resolution spectrometer (Princeton Instruments HRS-500, 0.05 nm resolution) to obtain the electron density (n_e) and electron temperature (T_e) in the dusty plasma. Dissociation of the hexane vapor in the reactive plasma produced an intense peak at 516 nm corresponding to the C_2 Swan band, and the ratio of intensities between the 516 nm peak and an Ar neutral line at 750 nm allowed us to qualitatively follow the reaction. The electron density in the dusty plasma was estimated by Stark broadening analysis of the H-β line at 486 nm [26], which in our case was readily observable from hexane precursor vapor dissociation. Briefly, Stark broadening refers to the Stark effect where electrical fields perturb the energy levels of an emitting atom [27]. In the case of a plasma, the electric fields are generated by the electrons and the field strength depends on the electron density in the local vicinity of the emitter. Of

particular relevance to this study, the resulting broadening of the emission line profile has been used to determine the average electron density in atmospheric-pressure plasmas [26,28,29].

The experimentally-measured H-β line is known to be a convolution of multiple broadening mechanisms in addition to the Stark effect. For this study, instrumental, Doppler, and van der Waals were found to be the other significant broadening mechanisms, with the instrumental contribution being the largest. The instrumental broadening was determined from a calibration with a mercury lamp. Both Doppler and van der Waals broadening depend on the gas temperature [26], which was obtained from fitting of molecular spectra. For the particle-free plasma, the OH emission band arising from some background water vapor contamination was used, and for the particle-containing plasma, the CH emission band arising from unreacted hexane vapor was used (see Supplementary Information). To obtain the Stark broadening contribution, the experimentally measured H-β line was fit to a Voigt profile, which is the convolution of Gaussian and Lorentzian broadening contributions. The contributions to the Gaussian width, the instrumental and Doppler broadening, were fit and subtracted to obtain the contributions to the Lorentzian width, the van der Waals and Stark broadening. Subtracting the van der Waals broadening then yielded the Stark broadening. Additional details of the analysis and a complete set of results are provided in the Supplementary Information, Table S7.

The mean electron temperature (T_e) was estimated from the Saha equation which relates the ionization state to the temperature and pressure for thermal plasmas [29,30]. For plasmas away from equilibrium, the Saha equation can be corrected, known as the Saha-Boltzmann equation, which introduces the population of states that is inferred from line ratios measured by OES. We solved the Saha-Boltzmann equation for several Ar ion-neutral line ratio combinations and found

that the estimated T_e did not vary widely, indicating that the system is close or at partial equilibrium. Details of this procedure are provided in the Supplementary Information, Table S8.

Constant number Monte Carlo simulations [18] (CNMC) were carried out to calculate the electron density and particle charge in a particle-producing plasma under the experimentally-measured environmental conditions. In general, CNMC is a stochastic computational approach used to investigate the evolution of a heterogeneous species undergoing chemical and physical reactions [31–33], in which the properties of a finite subset of the species (in this case, particles) are monitored, and system evolution is carried out by sampling reactions based on the probability of events during each time step. The properties of the nanoparticles for the simulations, including their diameters and concentrations, were extracted from experimental measurements (via IMS), assuming all particles were spherical. Specifically, 1000 individual nanoparticle diameters were sampled from a lognormal distribution with a geometric mean diameter of 36.0 nm and geometric standard deviation of 1.6, and the CNMC domain volume corresponded to a particle concentration of 2×10^6 cm^{-3}. Multiples of this particle concentration were also simulated to further investigate the effect of particles at higher number concentrations than that measured by experiments. Other plasma properties including ion density (and total negative charge density), electron temperature, and gas temperature summarized in Table 1 were provided by experimental measurements of the pristine atmospheric-pressure plasma formed in Ar and were kept constant. Particle charge states were monitored over time using rate equations for particle-electron [34] and particle-ion [20] collisions, which are applicable across a wide range of collisionality, and have shown strong agreement with experimental measurements of particle charge distributions in atmospheric-pressure aerosol systems [35]. We followed the methods of Smith and Matsoukas [18] for the time stepping procedure which are described in detail in the Supplementary Information. Briefly, each

particle-electron and particle-ion collision was assumed to lead to charge exchange and for each simulation time step, the electron concentration (C_e) was updated to maintain a quasi-neutral condition using the equation [2]:

$$C_e = C_{ion} + \frac{\sum z_p}{N} C_p \quad (2)$$

where C_{ion} and C_p are the ion and particle concentrations, respectively, z_p is the integer charge on individual particles in the simulation box, and N is the total number of particles in the simulation box. Simulations were carried out for 500 μs, after which time it was observed that all particle charge distributions remained constant (i.e. steady-state was achieved); charge distributions were evaluated by calculating the fraction of time each particle spent with a given charge state [36].

In support of experiments, a second set of CNMC simulations was also performed to address the potential influence of a molecular vapor species or nanocluster species on the plasma. As proof-of-concept, we assumed benzene-like sizes for such species, and sampled 10,000 nanometer-scale, ionizable entities each with a diameter of 0.66 nm and number concentrations of 1×10^{13} and 5×10^{13} cm^{-3}, corresponding to 2 ppm and 10 ppm, respectively. These concentrations were chosen based on how much leftover, unreacted hexane vapor or a molecular product that does not grow into nanoparticles might be present from the initial 80 ppm used to synthesize nanoparticles in the reactive plasma. In addition, we also found in experiments that the minimum concentration of hexane needed for particle nucleation was 50 ppm. Hence, these concentrations would not produce particles that could be detected via the instruments used here, consistent with our experiments (but have been observed in gas phase synthesis systems by more specialized mobility analyzers [37–39]). Collisions with electrons and ions were again assumed to lead to charge exchange with perfect efficiency, and the concentration of electrons was updated to ensure quasi-neutrality.

Table 1. Summary of plasma properties used as inputs for constant number Monte Carlo calculations obtained from experimental measurements on an RF-powered, atmospheric-pressure plasma formed in Ar.

Forward power (W)	Electron density (10^{14} cm^{-3})	Electron temperature (eV)	Gas temperature (K)
40	3.09	0.5	1350
50	3.40	0.5	1450
60	3.86	0.5	1620

III. Results and Discussion

Carbon was selected as the nanoparticle material for these studies because of its relatively high melting point and low sputtering yield, which we hoped would minimize evaporation or other potential undesired effects on the plasma. To verify the stability of the carbonaceous nanoparticles in the dusty plasma, we characterized the nanoparticles online by IMS and offline by collecting and performing TEM. Figures 2a and 2b show TEM images of nanoparticles collected with the dusty plasma off and with the dusty plasma on at an applied power of 60 W, respectively. The plasma off case represents the as-grown nanoparticles leaving the reactive plasma and allows a comparison of any morphology changes after further plasma interactions in the dusty plasma. The images show negligible differences in the morphology, which is more clearly confirmed by the higher magnification images (see insets of Figure 2a and 2b). The main difference is the deposited particle density, with a lower density for the dusty plasma on case, most likely from losses to the reactor walls by electrophoresis or thermophoresis.

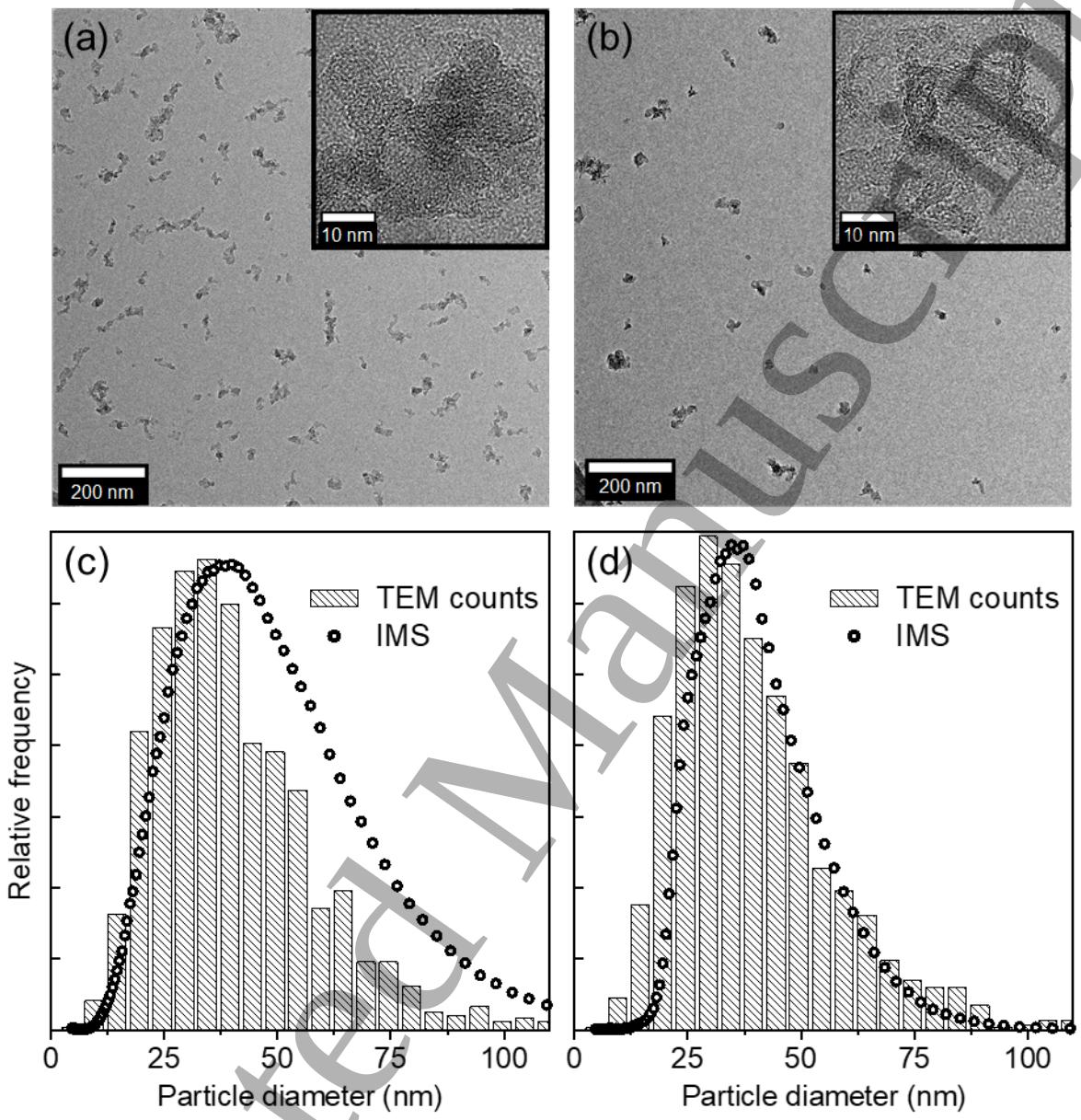

Figure 2. TEM images of **(a)** as-grown carbonaceous particles and **(b)** carbonaceous particles after dusty plasma exposure (60 W). Insets show high-magnification images of representative particles for each respective case. Diameter distributions of nanoparticles from TEM analysis and IMS measurements for **(c)** as-grown carbonaceous particles and **(d)** carbonaceous particles after dusty plasma exposure (60 W).

Other potential changes to the particles were assessed by comparing the diameter distributions of the nanoparticles. Figures 2c and 2d show the diameter distributions obtained from TEM analysis and IMS measurements of nanoparticles collected with the dusty plasma off and

with the dusty plasma on at an applied power of 60 W. TEM images were analyzed using ImageJ software and correspond to the apparent particle diameter, which we defined as the longest length measurable in 2D projections. Using this approximate diameter definition, good agreement is found between the TEM and IMS measurements, except at larger diameters for the as-grown nanoparticles (see Fig. 2c). IMS-inferred diameters are based upon application of the Stokes-Millikan equation [40] to link mobility to an (drag-equivalent) effective diameter; thus, for non-spherical particles and aggregates it yields a size representative of the overall aggregate architecture. Aggregates do appear to be present in TEM images, and for any aggregates present, there would be disagreement between the IMS-inferred diameters and TEM-inferred diameters. Aggregation hence likely explains the slight disagreement between TEM and IMS distributions at the outlet of the reactive plasma. Excellent agreement is observed in the distributions shown in Fig 2d. We suggest that this is due to modest amounts of sintering and restructuring in the second plasma that produces more spherical, densified particles. Prior studies have demonstrated that particle heating via collisions with plasma species can lead to crystallization [11] and evaporation [12].

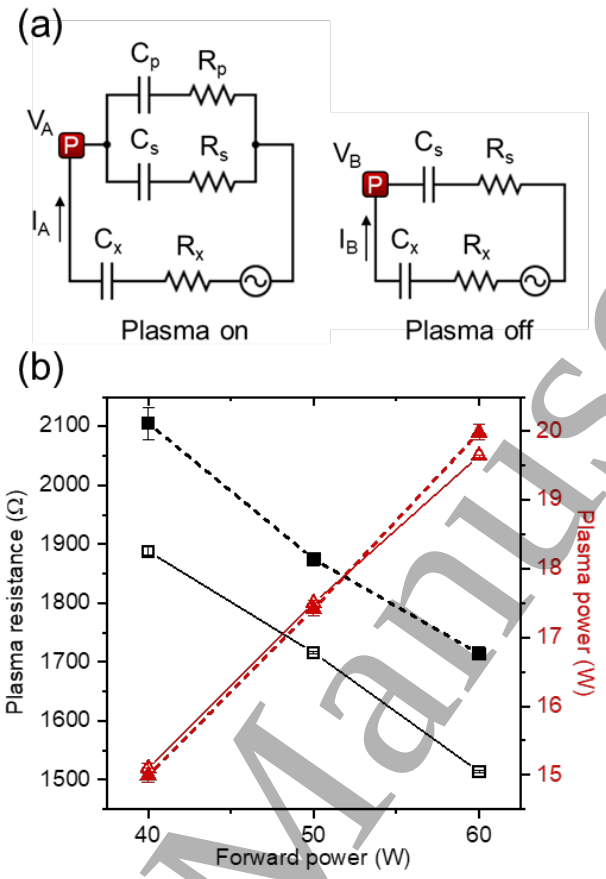

Figure 3. (a) Equivalent circuit diagrams of the dusty plasma reactor for "plasma on" and "plasma off" cases. p=plasma, s=stray, and x=transmission. V_A and I_A are the voltage and current for the plasma on case; V_B and I_B are for the plasma off case. **(b)** Plasma resistances (squares) and plasma powers (triangles) as a function of forward RF power. The filled and unfilled symbols correspond to Ar only and particle-containing conditions, respectively.

The main effect expected from interactions of nanoparticles and a plasma is attachment of the higher energy electrons to the particles. To characterize this effect, we measured the electron density, n_e, in the dusty plasma, first by electrical probe. Figure 3a shows a schematic diagram of the simple equivalent circuit used to model the plasma on and plasma off and measure the current and voltage with the probe, represented as "P". For the plasma *off* condition, we neglected any capacitance attributed to the plasma-side of the circuit. Figure 3b shows the measured plasma resistance, R_p, and power in the dusty plasma with only inert Ar (for comparison) and with

carbonaceous nanoparticles at a concentration of 2.0×10^{6} cm^{-3}. The plasma powers were almost identical at all forward RF powers tested which shows that the presence of particles had a minimal effect on the power transmission. The estimated electron densities are 3.86×10^{14} cm^{-3} and 3.41×10^{14} cm^{-3} for the Ar only and particle-containing conditions at 60 W, respectively. The decrease in electron density of ~4×10^{13} cm^{-3} with the introduction of nanoparticles appears to be consistent with the predicted electron attachment and previous studies of low-pressure dusty plasmas. The complete set of data is shown in the Supplementary Information, Tables S1-S5.

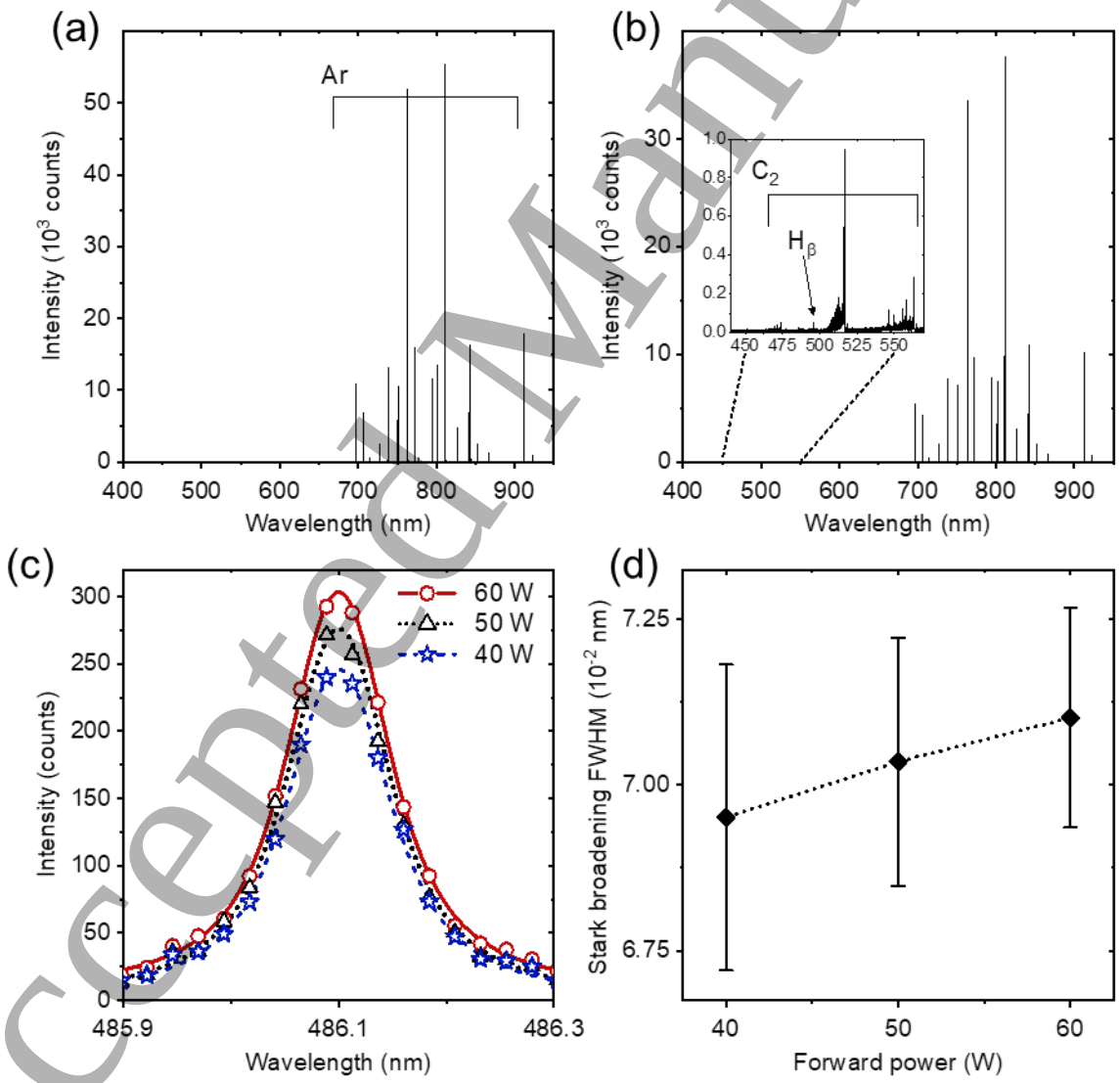

Figure 4. (a) Optical emission spectrum of particle-free plasma (Ar only) showing only Ar lines. **(b)** Optical emission spectrum of particle-containing plasma showing Ar and carbon species lines.

Inset shows close-up of C_2 Swan band. **(c)** Optical emission spectrum of particle-containing plasma showing H-β (486 nm) line at various powers. **(d)** Full-width-at-half-maximum (FWHM) values of H-β emission line corresponding to Stark broadening obtained by deconvolution. Error bars correspond to the variance associated with the Voigt fit to the experimental data.

To support the electrical probe measurements and analysis, we also obtained electron density values by Stark broadening analysis as well as general qualitative observations via OES. Emission spectra of the dusty plasma with only inert Ar (for comparison) and with carbonaceous nanoparticles at a concentration of 2.0×10^6 cm^{-3} are shown in Figures 4a and 4b, respectively. The main difference is features corresponding to CH and C_2 observed in the 300-600 nm range, more clearly shown in the inset of Figure 4b. The presence of these species indicates that there is some unreacted hexane vapor or other molecular reaction by-products from the reactive plasma entering the dusty plasma. It may also be possible that there is some small amount of nanoparticle evaporation that could not be ruled out by particle characterization, which we will address later. As shown in Figure 4c, the H-β line at 486 nm is also observed which allows the electron density to be estimated by Stark broadening analysis without adding any additional hydrogen source such as H_2 gas. Figure 4d shows the FWHM of the contribution from only the Stark effect after deconvolution and analysis. Using correlations [26], the electron density is estimated for the particle-containing dusty plasma to be ~2.1×10^{14} cm^{-3}, which is in good agreement with electrical probe measurements. However, we observed that the broadening did not vary widely with applied power and this may be due to the changes in electron density being on the same order of magnitude as the lower limit of the Stark broadening technique [26]. We note that the electron density of a particle-free plasma could not be obtained by Stark broadening since there is no hexane vapor and therefore, no H-β emission.

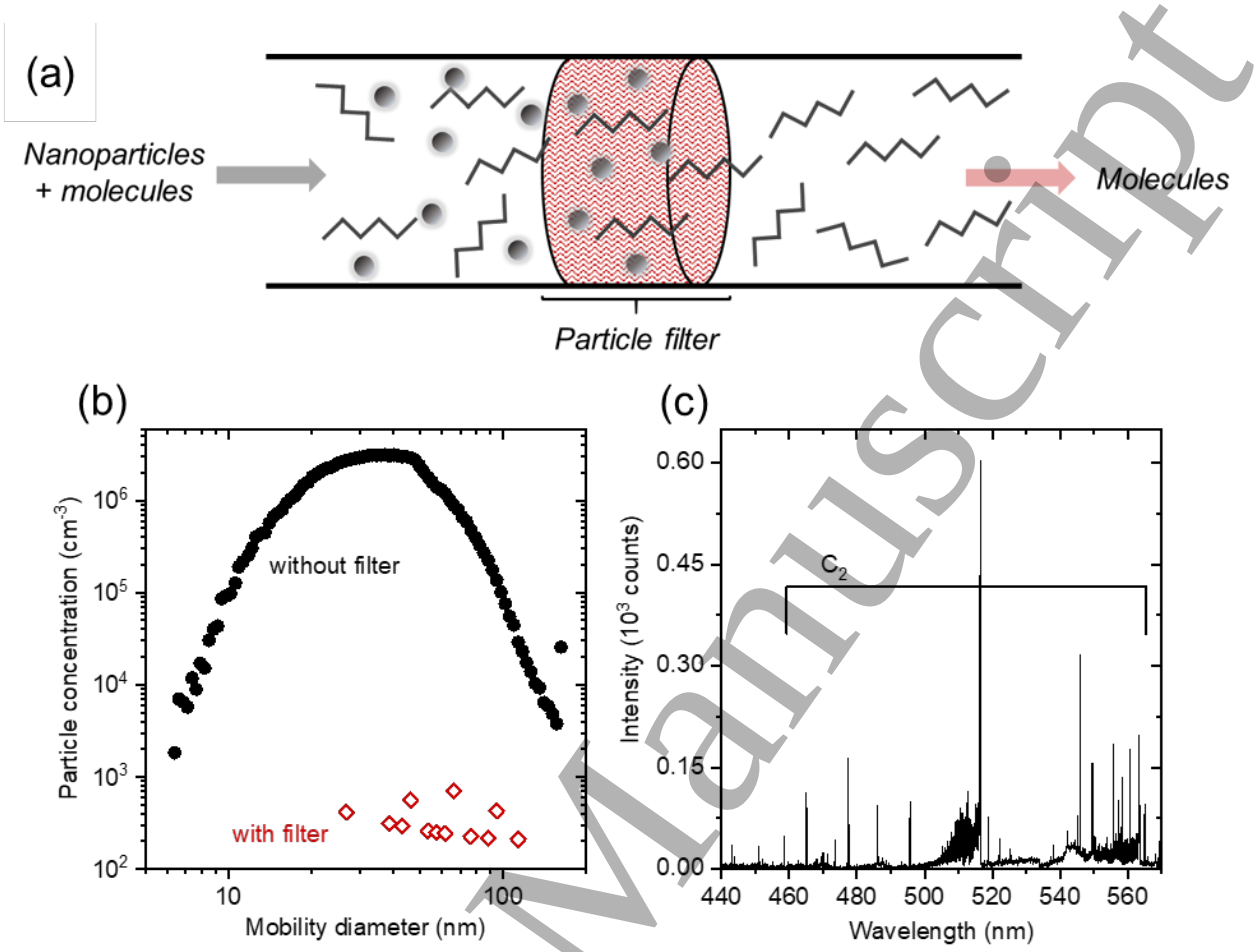

Figure 5. (a) Illustration depicting inline filtration of nanoparticles between the reactive and dusty plasma reactors. **(b)** Mobility diameter distributions measured with and without inline filter by IMS after dusty plasma (60 W). **(c)** Optical emission spectrum of dusty plasma with inline filter showing carbon species lines (C_2 Swan band).

The nanoparticles were introduced in the dusty plasma directly from the effluent of the reactive plasma, which as indicated by OES, could also contain unreacted hexane vapor or other molecular reaction by-products. To isolate the effect of the nanoparticles from these other molecular species, a control experiment illustrated in Figure 5a was designed with a filter inline between the reactive and dusty plasmas to remove the nanoparticles before the dusty plasma. The removal of the nanoparticles by the filter was confirmed by IMS as shown in Figure 5b. We note that for this measurement, the dusty plasma was on and also shows that no new nanoparticles were nucleated from any unreacted hexane vapor or molecular products; based on our experiments in

the reactive plasma, this indicates that the concentration of any molecular vapor was less than 50 ppm, the minimum hexane vapor concentration required for particle nucleation. Emission spectroscopy of the dusty plasma showed the presence of CH and C_2 species, which confirms that there are molecular vapor species in the reactive plasma effluent. Since these lines are observed even without nanoparticles and are of comparable intensity (see inset of Fig. 4b), particle evaporation is an unlikely reason for these species.

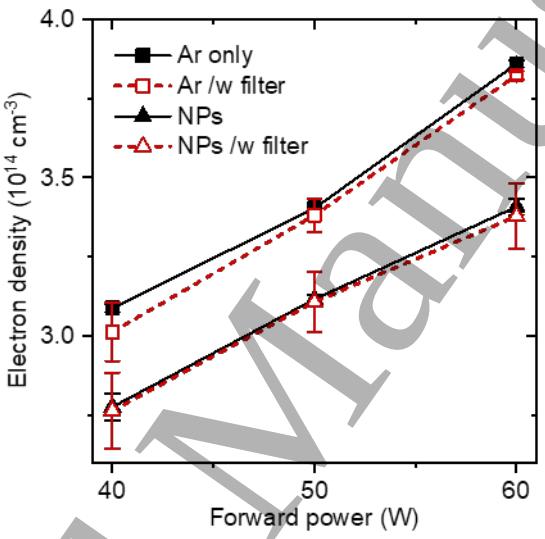

Figure 6. Electron densities measured by power probe for various conditions in the dusty plasma reactor: particle-free (Ar only), nanoparticles (NPs) produced in the reactive plasma, particle-free with inline filter (Ar only), and nanoparticles (NPs) produced in the reactive plasma with inline filter.

Figure 6 shows all the electron densities calculated from electrical probe data in the dusty plasma reactor for the Ar only case and the particle-containing case with and without an inline filter. For completion, we also measured the electron density with an inline filter for the Ar only case even though no nanoparticles were synthesized in the reactive plasma. Overall, the electron densities are found to increase with power for all cases, as would be expected [24], from 3.09×10^{14} cm^{-3} at 40 W to 3.86×10^{14} cm^{-3} at 60 W for the pristine, particle-free environment, and 2.78×10^{14} cm^{-3} at 40 W to 3.41×10^{14} cm^{-3} 60 W for the particle-containing environment. Negligible difference is found between the electron densities for a particle-free environment with and without

an inline filter. More surprisingly, while the electron density is lower for the particle-containing plasma, it is also equally lower with the inline filter. We stress that there are two important conclusions from the overlap of these two experiments: one, the nanoparticles do not contribute to an electron density decrease and two, a molecular vapor species that leaves the reactive plasma but is not removed by the filter appears to be responsible for the electron density decrease.

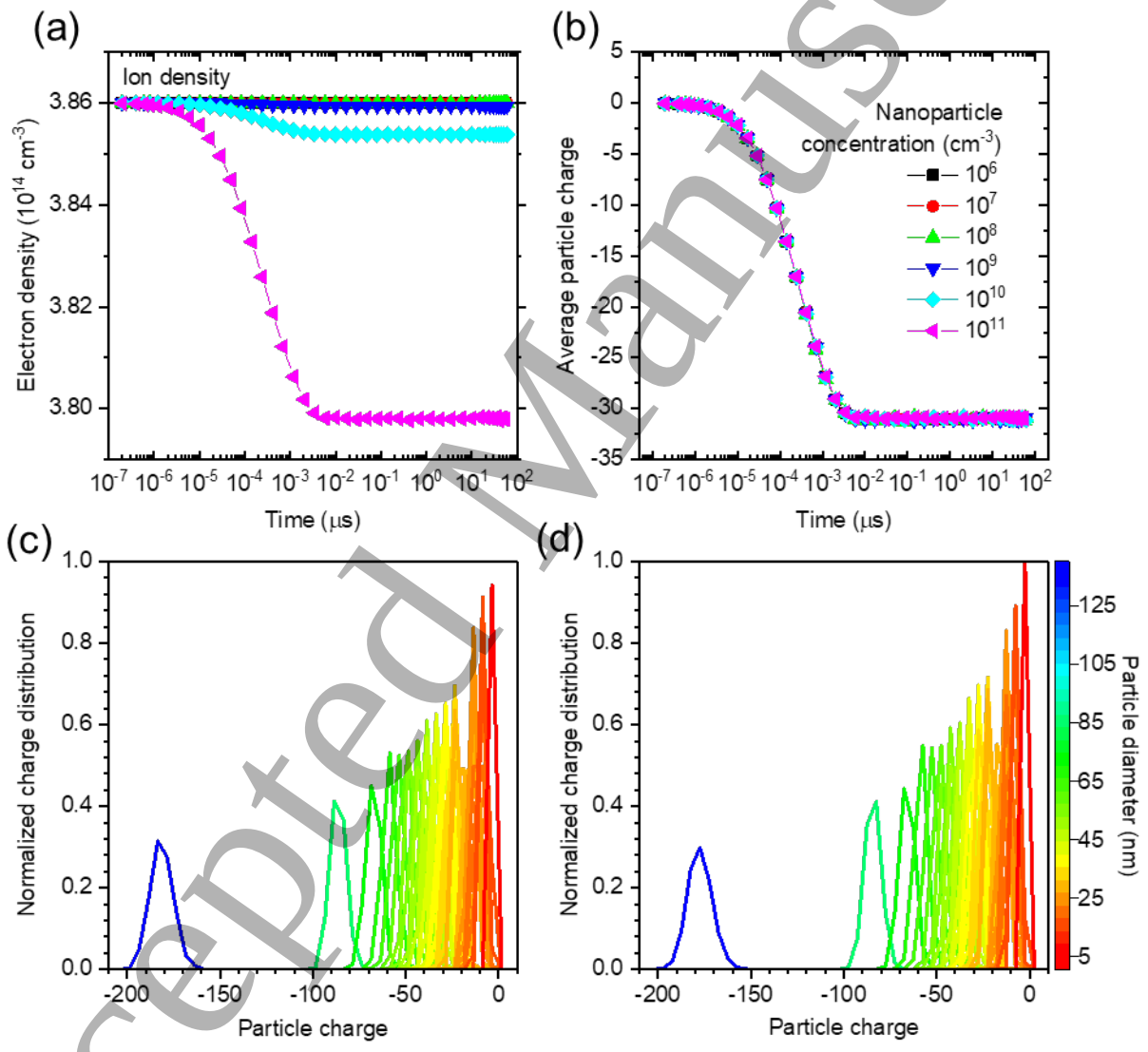

Figure 7. Calculations from simulations of particle-containing, atmospheric-pressure plasma for **(a)** electron density and **(b)** average charge on nanoparticle as a function of residence time in the plasma at different particle concentrations where 10^6 cm^{-3} represents the experimentally-measured value. The legend shown in **(b)** applies to **(a)**. Time-averaged charge distribution of particle at a specific diameter indicated by the color for **(c)** particle-free plasma, and **(d)** particle-containing plasma. Electron densities and particle concentrations in **(c-d)** are the same as experiments.

We performed CNMC simulations to support the experimental measurements of the particle-containing, atmospheric-pressure Ar plasma systems. It is well-established that nanoparticles acquire negative charge states in plasma environments [41–43], with the average charge increasing in magnitude with increasing particle diameter. Therefore, it is plausible that a population of nanoparticles would deplete electrons in a dusty plasma. Figure 7a shows that for the nanoparticle diameter and concentration present in the atmospheric-pressure plasma studied here, simulations find no discernable difference in the electron densities between the particle-free and particle-containing case. If and only if the nanoparticle concentrations are a factor of 10^5 times higher than those found in experiments would the electron density in the atmospheric-pressure plasma be affected; in the simulations, we purposefully chose a particle concentration that would lead to the observed degree of reduction in electron density (see Fig. 6). For all simulated conditions, the simulations confirm that the nanoparticles present in the plasma would be highly negatively charged as shown by the average particle charge state (over the entire size distribution) in Fig. 7b. As a function of simulation time, the average charge initially decreases rapidly, as all particles are initiated with a neutral charge state, and the system reaches steady-state after 10^{-2} μs. At steady-state, the average charge remains near -32 regardless of the particle concentration, further confirming that the dusty particle concentration would need to be near 1.4×10^{12} cm^{-3}, ~10^5 times the actual particle concentration to match the reduction of electron density observed in experiments. Figures 7c and 7d show the charge distributions for selected particle diameters calculated from simulations for the experimentally-measured electron densities in the particle-free and the particle-containing plasma at 60 W. In agreement with prior calculations [43], the average charge increases in magnitude with increasing size, confirming that the measured reduction in

electron density in the particle-containing plasma case has negligible effect on the particle charge distributions.

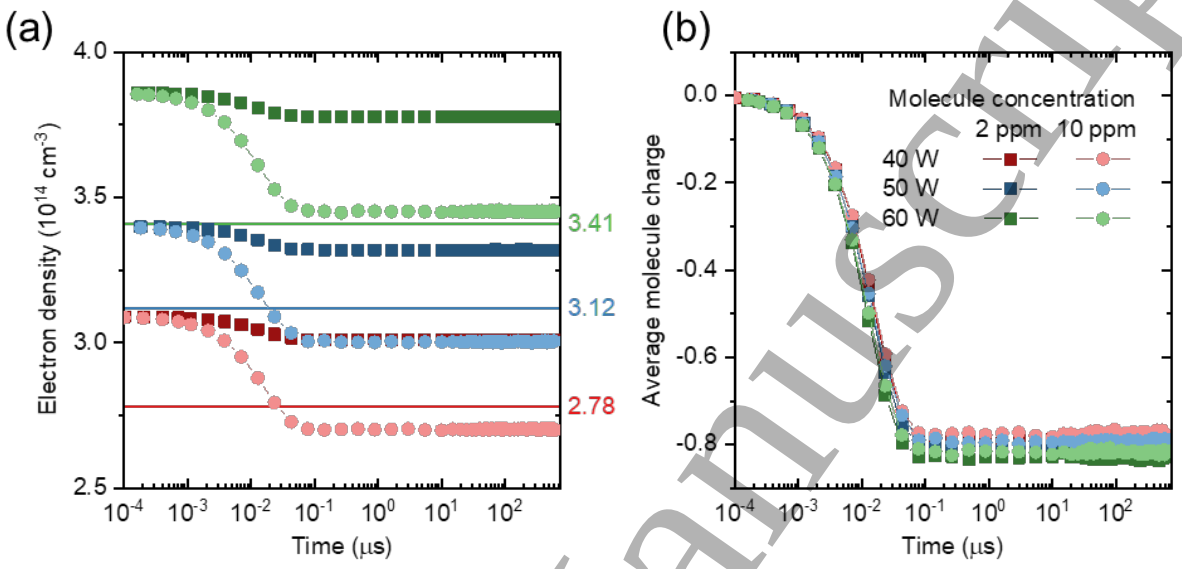

Figure 8. Calculations from simulations of molecular vapor-containing atmospheric-pressure plasma for **(a)** electron density and **(b)** average charge as a function of residence time in the plasma at various powers and concentrations of an ionizable molecule. Electron densities from experimental measurements of the dusty plasma with nanoparticles produced in the reactive plasma and an inline filter are shown in **(a)** for reference. The legend shown in **(b)** applies to **(a)**.

In support of our control experiment with the inline filter which suggested that a molecular vapor species is responsible for the reduction in electron density in the dusty plasma, we also performed similar CNMC simulations with an ionizable molecular species to roughly represent a molecular vapor species leaving the reactive plasma. Figure 8a shows electron densities calculated as a function of simulation time for a plasma containing 1×10^{13} cm^{-3} (2 ppm) and 5×10^{13} cm^{-3} (10 ppm) of benzene. For comparison, solid lines are included for the experimentally-measured reduction in electron densities at each condition. Excellent agreement is found between the steady-state electron density calculated from simulations at 5×10^{13} cm^{-3} and experimental measurements, which has two ramifications. One, the simulations confirm that it is possible for a molecular-scale electronegative species to lead to a reduction in electron density in an atmospheric-pressure plasma,

i.e., the species becomes negatively charged and depletes electrons. The charge levels are relatively low, with a mean charge near -0.8 for all simulated concentrations as shown in Fig. 8b. Two, the simulations indicate that the concentration of the molecular species must be relatively high, ~10 ppm, relative to the initial precursor vapor concentration in the reactive plasma which was ~80 ppm. The most likely species are the precursor itself, unreacted in the reactive plasma, evaporated material from particles (unlikely in the case of carbon), or a highly favorable reaction by-product that does not further grow into particles. Overall, the importance of the molecular vapor species suggests that in many respects, particle-producing plasmas may contain features akin to electronegative plasmas [44].

Realizing that typical conditions for particle growth in atmospheric pressure plasmas lead to minimal direct influence of particles on plasma species, while low-pressure synthesis conditions yield particles in concentrations which have been shown to directly impact electron densities, we now provide a unifying picture of electron depletion in dusty plasmas across a wide range of pressures, electron densities, and particle diameters. Assuming an ideal monodisperse particle size distribution, we first calculate the equilibrium particle charge for a range of nanoparticle diameters, 1 to 1000 nm, by CNMC simulations, shown in Fig. 9a. Representative plasma parameters including electron density, electron temperature, gas temperature, and background pressure were chosen for the calculations: 10^{10} cm^{-3}, 3 eV, 300 K, and 1 Pa for low-pressure Ar plasmas [2] and 10^{14} cm^{-3}, 1 eV, 1000 K, and 10^{5} Pa for atmospheric-pressure Ar plasmas [3]. We note that charge limiting mechanisms were ignored, such as electron desorption or thermionic emission, and therefore, the calculations represent the maximum impact of particles on electron depletion.

Next, the particle charge was used to calculate the electron density change by applying a charge balance:

$$n_e = n_e^0 - Q_p n_p = n_i - Q_p n_p \quad (3)$$

where n_e^0 is the initial particle-free electron density, n_p is the particle concentration, and n_i is the ion density and assumed to be equal to the initial or clean, particle-free electron density (quasineutrality). We now introduce a term that corresponds to the fractional degree of depletion of the electron density based on the initial particle-free electron density, η, such that 100% corresponds to all of the electrons being captured by the particles:

$$\eta = \frac{n_e^0 - n_e}{n_e^0} = \frac{Q_p n_p}{n_e^0} \quad (15)$$

Figure 9b shows the initial electron density-to-particle concentration ratio, n_e^0/n_p, versus particle diameter for various η: 1%, 10%, and a maximum limit that serves as a demarcation between a "stable" and "unstable" plasma. The range of values correspond to those in the particle charge calculations. In principle, significant depletion of electrons from the bulk plasma occurs when the ratio approaches 1, and as expected, due to a higher degree of charging (see Fig. 9a), larger particles lead to more severe electron depletion for a given n_e^0/n_p in both high and low pressure environments. The maximum limit was chosen based on Whipple *et al.* who determined that the minimum ratio of electron to ion number density in a dusty plasma is equal to $\sqrt{m_e/m_i}$, and below this critical value the plasma will extinguish [45]. For an Ar plasma, this limit is 99.7% which means that for the plasma state to persist, at least 0.3% of the initial electron density must be preserved.

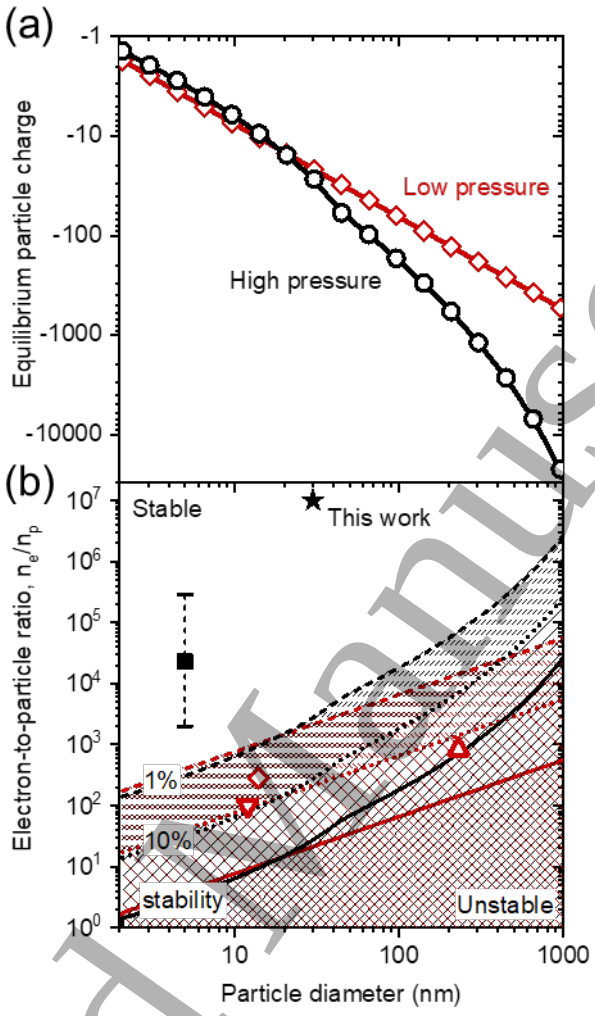

Figure 9. (a) Equilibrium particle charge calculated as a function of particle diameter for high (black) and low (red) pressure plasma conditions. The high and low pressure conditions were chosen as 10^5 and 1 Pa respectively. **(b)** Electron-to-nanoparticle concentration ratio calculated as a function of particle diameter for high (black) and low (red) pressure plasma conditions. Lines are shown demarcating intermediate degrees of electron depletion (1%, 10%) and a theoretical maximum denoted by the solid line labeled 'stability'. The following values from the literature are shown as points, where filled symbols indicate atmospheric pressure and unfilled symbols indicate low pressure environments: *this work* (star), Askari *et al.*[16] (square), Woodard *et al.* 2018[14] (diamond) and 2020 [46] (point-down triangle), and Bouchoule and Boufendi 1993[47] (point-up triangle).

We are aware that there may be other effects that arise from nanoparticles and electron depletion on the collective behavior of dusty plasmas such as an increase in electron temperature [48], and we have neglected these more complex effects for the sake of simplicity. Nonetheless, the effects on electron density provide important guidelines for the design of plasma synthesis

reactors in terms of nanoparticle size and number concentration at a given operating pressure. In Fig. 9b, we also show previously published results for various dusty plasmas (Askari *et al.* [16], Woodard *et al.* 2018 [14] and 2020 [46], and Bouchoule and Boufendi 1993 [47]). The studies at low pressure are found to lie in a transition regime between stable and unstable where the electron density decreases by ~10%. Our current work appears safely in the stable regime with virtually no change to the electron density. One other atmospheric pressure study is included, although particle concentrations were not measured [16]. A range of possible electron-to-particle ratios was calculated from the silane concentration for different conversions, indicated by the error bars, and even at 100% conversion the depletion was < 1%.

Our findings show that one of the important design considerations for nanoparticle synthesis by atmospheric-pressure plasmas is unreacted vapor precursor and/or precursor conversion to molecular products. We suspect that the n_e^0/n_p (initial electron density-to-particle concentration ratio) is likely too high at atmospheric pressure to ever allow the synthesized nanoparticles to make their presence in the plasma felt. On the other hand, ionizable molecular entities may exist in sufficiently high enough concentrations to disturb the plasma, ultimately affecting the nucleation and growth of the nanoparticles. Molecular species could similarly impact low-pressure plasmas, as has been previously reported for hydrocarbon plasmas [49], but in this case, there would be a cumulative effect with nanoparticles since their n_e^0/n_p is typically lower. We note that the background gas may be another factor that impacts the effect of the nanoparticles and molecular vapor on the plasma. We expect similar effects to what was found here for other noble, electropositive gases such as helium and neon. However, the effect may change for electronegative gases where the composition of the charged species is different with both positively- and negatively-charged ions in addition to the negatively-charged electrons.

IV. Conclusions

We have applied non-contact diagnostics to a tandem, flow-through plasma system and performed CNMC simulations to understand the effect of nanoparticles on realistic, particle-producing plasmas at atmospheric pressure. The results indicate that while there is a decrease in the electron density, the origin is a residual molecular vapor species and not the nanoparticles. The finding is distinct from low-pressure dusty plasmas and shows that at atmospheric-pressure, particle concentrations would have to be exceedingly high ($>10^{12}$ cm^{-3}) to impact the electron density. In comparison, a reasonable amount of residual molecular vapor either in the form of unreacted precursor or a reaction by-product is more likely to deplete electrons. Future studies are required to more carefully identify the molecular vapor species and characterize its charging behavior.

Acknowledgments

This work was supported by the Department of Energy under Grant No. DE-SC0018202.

References

[1] Selwyn G S 1993 A phenomenlogical study of particulates in plasma tools and processes *Jpn. J. Appl. Phys.*

[2] Kortshagen U R, Sankaran R M, Pereira R N, Girshick S L, Wu J J and Aydil E S 2016 Nonthermal plasma synthesis of nanocrystals: Fundamental principles, materials, and applications *Chem. Rev.* **116** 11061–127

[3] Mariotti D and Sankaran R M 2010 Microplasmas for nanomaterials synthesis *J. Phys. D. Appl. Phys.*

[4] Kramer N J, Aydil E S and Kortshagen U R 2015 Requirements for plasma synthesis of nanocrystals at atmospheric pressures *J. Phys. D. Appl. Phys.* **48**

[5] Kersten H, Deutsch H, Stoffels E, Stoffels W W, Kroesen G M W and Hippler R 2001 Micro-disperse particles in plasmas: From disturbing side effects to new applications *Contrib. to Plasma Phys.*

[6] Fortov V E, Ivlev A V., Khrapak S A, Khrapak A G and Morfill G E 2005 Complex (dusty) plasmas: Current status, open issues, perspectives *Phys. Rep.*

[7] Shukla P K 2001 A survey of dusty plasma physics *Physics of Plasmas*

[8] Goree J 1994 Charging of particles in a plasma *Plasma Sources Sci. Technol.* **3** 400–6

[9] Khrapak S A, Ratynskaia S V., Zobnin A V., Usachev A D, Yaroshenko V V., Thoma M H, Kretschmer M, Höfner H, Morfill G E, Petrov O F and Fortov V E 2005 Particle charge in the bulk of gas discharges *Phys. Rev. E - Stat. Nonlinear, Soft Matter Phys.*

[10] Mangolini L and Kortshagen U 2009 Selective nanoparticle heating: Another form of nonequilibrium in dusty plasmas *Phys. Rev. E - Stat. Nonlinear, Soft Matter Phys.*

[11] Kramer N J, Anthony R J, Mamunuru M, Aydil E S and Kortshagen U R 2014 Plasma-induced crystallization of silicon nanoparticles *J. Phys. D. Appl. Phys.* **47**

[12] Uner N B and Thimsen E 2017 In-Flight Size Focusing of Aerosols by a Low Temperature Plasma *J. Phys. Chem. C*

[13] Bilik N, Anthony R, Merritt B A, Aydil E S and Kortshagen U R 2015 Langmuir probe measurements of electron energy probability functions in dusty plasmas *J. Phys. D. Appl. Phys.*

[14] Woodard A, Shojaei K, Nava G and Mangolini L 2018 Langmuir probe characterisation of an Ar-H2 non-thermal plasma loaded with carbon nanoparticles *Plasma Sources Sci. Technol.*

[15] Chiang W H, Mariotti D, Sankaran R M, Eden J G and Ostrikov K 2019 Microplasmas for Advanced Materials and Devices *Adv. Mater.*

[16] Askari S, Levchenko I, Ostrikov K, Maguire P and Mariotti D 2014 Crystalline Si nanoparticles below crystallization threshold: Effects of collisional heating in non-thermal atmospheric-pressure microplasmas *Appl. Phys. Lett.* **104**

[17] Cole J, Zhang Y, Liu T, Liu C J and Sankaran R M 2017 Process scale-up considerations for non-thermal atmospheric-pressure plasma synthesis of nanoparticles by homogenous nucleation *J. Phys. D. Appl. Phys.*

[18] Smith M and Matsoukas T 1998 Constant-number Monte Carlo simulation of population balances *Chem. Eng. Sci.*

[19] Gopalakrishnan R and Hogan C J 2012 Coulomb-influenced collisions in aerosols and dusty plasmas *Phys. Rev. E - Stat. Nonlinear, Soft Matter Phys.* **85**

[20] Chahl H S and Gopalakrishnan R 2019 High potential, near free molecular regime Coulombic collisions in aerosols and dusty plasmas *Aerosol Sci. Technol.*

[21] Mangolini L, Thimsen E and Kortshagen U 2005 High-yield plasma synthesis of luminescent silicon nanocrystals *Nano Lett.*

[22] Chen D R, Pui D Y H, Hummes D, Fissan H, Quant F R and Sem G J 1998 Design and evaluation of a nanometer aerosol differential mobility analyzer (Nano-DMA) *J. Aerosol Sci.*

[23] Zhu X M, Pu Y K, Balcon N and Boswell R 2009 Measurement of the electron density in atmospheric-pressure low-temperature argon discharges by line-ratio method of optical

emission spectroscopy *J. Phys. D. Appl. Phys.* **42**

[24] Lieberman M A and Lichtenberg A J 2005 *Principles of Plasma Discharges and Materials Processing: Second Edition*

[25] Raizer Y P 1991 *Gas Discharge Physics* ed J E Allen (Berlin, Germany: Springer-Verlag Berlin Heidelberg)

[26] Laux C O, Spence T G, Kruger C H and Zare R N 2003 Optical diagnostics of atmospheric pressure air plasmas *Plasma Sources Sci. Technol.* **12** 125–38

[27] Gigosos M A, González M Á and Cardeñoso V 2003 Computer simulated Balmer-alpha, -beta and -gamma Stark line profiles for non-equilibrium plasmas diagnostics *Spectrochimica Acta - Part B Atomic Spectroscopy*

[28] Du B, Sadeghi N, Tsankov T V., Luggenhölscher D and Czarnetzki U 2012 Temporally resolved optical emission spectroscopic investigations on a nanosecond self-pulsing micro-thin-cathode discharge *Plasma Sources Sci. Technol.*

[29] Balcon N, Aanesland A and Boswell R 2007 Pulsed RF discharges, glow and filamentary mode at atmospheric pressure in argon *Plasma Sources Sci. Technol.* **16** 217–25

[30] Ochkin V N 2009 *Spectroscopy of Low Temperature Plasma* (Wiley-VCH)

[31] Mukherjee D, Sonwane C G and Zachariah M R 2003 Kinetic Monte Carlo simulation of the effect of coalescence energy release on the size and shape evolution of nanoparticles grown as an aerosol *J. Chem. Phys.*

[32] Kruis F E, Maisels A and Fissan H 2000 Direct simulation Monte Carlo method for particle coagulation and aggregation *AIChE J.*

[33] Maisels A, Kruis F E and Fissan H 2004 Coagulation in bipolar aerosol chargers *J. Aerosol Sci.*

[34] Allen J E 1992 Probe theory - the orbital motion approach *Phys. Scr.*

[35] Li L, Chahl H S and Gopalakrishnan R 2020 Comparison of the predictions of Langevin Dynamics-based diffusion charging collision kernel models with canonical experiments *J. Aerosol Sci.*

[36] Gopalakrishnan R, Meredith M J, Larriba-Andaluz C and Hogan C J 2013 Brownian dynamics determination of the bipolar steady state charge distribution on spheres and non-spheres in the transition regime *J. Aerosol Sci.*

[37] Kumar A, Kang S, Larriba-Andaluz C, Ouyang H, Hogan C J and Sankaran R M 2014 Ligand-free Ni nanocluster formation at atmospheric pressure via rapid quenching in a microplasma process *Nanotechnology*

[38] Vazquez-Pufleau M, Wang Y, Biswas P and Thimsen E 2020 Measurement of sub-2 nm stable clusters during silane pyrolysis in a furnace aerosol reactor *J. Chem. Phys.*

[39] Domaschke M, Lübbert C and Peukert W 2019 Analysis of ultrafine metal oxide particles in aerosols using mobility-resolved time-of-flight mass spectrometry *J. Aerosol Sci.*

[40] Zhang C, Thajudeen T, Larriba C, Schwartzentruber T E and Hogan C J 2012 Determination of the scalar friction factor for nonspherical particles and aggregates across the entire knudsen number range by Direct Simulation Monte Carlo (DSMC) *Aerosol Sci. Technol.*

[41] Khrapak S A, Morfill G E, Khrapak A G and D'Yachkov L G 2006 Charging properties of a dust grain in collisional plasmas *Phys. Plasmas*

[42] Gatti M and Kortshagen U 2008 Analytical model of particle charging in plasmas over a wide range of collisionality *Phys. Rev. E - Stat. Nonlinear, Soft Matter Phys.* **78**

[43] Matsoukas T, Russell M and Smith M 1996 Stochastic charge fluctuations in dusty plasmas *J. Vac. Sci. Technol. A Vacuum, Surfaces, Film.*

[44] Franklin R N 2002 Electronegative plasmas - Why are they so different? *Plasma Sources Science and Technology*

[45] Whipple E C, Northrop T G and Mendis D A 1985 The electrostatics of a dusty plasma *J. Geophys. Res. Sp. Phys.*

[46] Woodard A, Shojaei K, Berrospe-Rodriguez C, Nava G and Mangolini L 2020 Electron emission from particles strongly affects the electron energy distribution in dusty plasmas *J. Vac. Sci. Technol. A*

[47] Bouchoule A and Boufendi L 1993 Particulate formation and dusty plasma behaviour in argon-silane RF discharge *Plasma Sources Sci. Technol.*

[48] Bouchoule A and Boufendi L 1994 High concentration effects in dusty plasmas *Plasma Sources Sci. Technol.* **3** 292–301

[49] Baby A, Mahony C M O and Maguire P D 2011 Acetylene-argon plasmas measured at a biased substrate electrode for diamond-like carbon deposition: I. Mass spectrometry *Plasma Sources Sci. Technol.*